Journal of Physics: Condensed Matter

PAPER

Graphene oxide and its derivatives as potential Ovchinnikov ferromagnets

To cite this article: Apurva Sinha *et al* 2021 *J. Phys.: Condens. Matter* **33** 375801

View the article online for updates and enhancements.

You may also like

- Design of a Class of New $sp^2 – sp^3$ Carbons Constructed by Graphite and Diamond Building Blocks
Kun Luo, , Bing Liu et al.
- Reversible synthesis of GO: Role of differential bond structure transformation in fine-tuning photodetector response
Abgeena Shabir, Abid, Poonam Sehrawat et al.
- Theoretical model of structure-dependent conductance crossover in disordered carbon
Mikhail V. Katkov and Somnath Bhattacharyya

This content was downloaded from IP address 220.158.144.60 on 18/07/2023 at 19:53

IOP Publishing Journal of Physics: Condensed Matter
J. Phys.: Condens. Matter **33** (2021) 375801 (11pp) https://doi.org/10.1088/1361-648X/ac0d84

Graphene oxide and its derivatives as potential Ovchinnikov ferromagnets

Apurva Sinha[1,*], Pranay Ranjan[2], Anzar Ali[3], Jayakumar Balakrishnan[4,*] and Ajay D Thakur[1,*]

[1] Department of Physics, Indian Institute of Technology, Patna, Bihta 801106, India
[2] Department of Physics, UAE University, Al-Ain 15551, United Arab Emirates
[3] Department of Physics, Indian Institute of Science Education and Research, Mohali 140306, India
[4] Department of Physics, Indian Institute of Technology Palakkad, Kozhippara 678557, India

E-mail: apurva.pph16@iitp.ac.in, jayakumar@iitpkd.ac.in and ajay.thakur@iitp.ac.in

Received 25 April 2021, revised 7 June 2021
Accepted for publication 22 June 2021
Published 9 July 2021

Abstract

Ovchinnikov postulated the possibility of ferromagnetism in organic compounds having a mixed density of sp^3 and sp^2 carbon atoms. Such systems provide an interesting avenue for exploring magnetism in the absence of the quintessential d- and f-block elements as ingredients. As graphene oxide (GO) and its derivatives naturally possess a mixture of sp^3 and sp^2 carbon atoms, it is pertinent to look at them as potential candidates for Ovchinnikov ferromagnetism. We have looked at the evolution of magnetic property in a series of GO samples with a gradual increase in the degree of oxidation and hence the sp^3/sp^2 fraction. Starting with a GO sample with a high sp^3/sp^2 ratio, we utilize chemical reduction technique to prepare another set of reduced graphene oxide (rGO) samples. Magnetization measurements on these samples further illustrate the importance of sp^3/sp^2 fraction on magnetic behavior suggesting GO and its derivatives as a potential Ovchinnikov ferromagnet candidate. The evolution of magnetic moment with sp^3/sp^2 carbons can be utilized in carbon based spintronic applications.

Keywords: graphene oxide, reduced graphene oxide, Ovchinnikov ferromagnet, magnetism

Supplementary material for this article is available online

(Some figures may appear in colour only in the online journal)

1. Introduction

Over the last few decades, magnetism in carbon based systems like graphene, graphene oxide (GO), reduced graphene oxide (rGO) etc have remained an important subject of interest. It is because of their unexpected tendency to show ferromagnetic (FM) property, even at room temperature [1–4]. Despite they lack d or f electrons which are the key components of the traditional ferromagnets, they have shown potential magnetic applications in various fields like spintronics [5], imaging and biomedicine [6], electrode and adsorbent [7], water cleaning [8], dye adsorption [9] etc. This led to an exclusive search for the source of unpaired spins in carbon based systems [10]. Several factors responsible for the creation of unpaired spins in such systems reported are vacancies or nanoholes [11–13], topological defects [14–16], Stone–Wales defects [17], pentagon–octagon pairs [18], temperature dependence [19], edge states [20, 21], adatoms [22–25], disordered and functionalized regions [26–28], individual oxygen functional groups (OFGs) dependent magnetism [16, 27, 29–37] etc. Interesting applications of magnetic nanoparticles decorated composite of carbon based systems have been demonstrated recently [38]. In this paper we have tried a detailed analysis of magnetism in a set of samples of GO and rGO. We assume the mixed density of sp^3 and sp^2 carbons in them as the main source of unpaired

* Authors to whom any correspondence should be addressed.

 © 2021 IOP Publishing Ltd Printed in the UK

spins and an exchange interaction between the π electrons and the unpaired spins results into the net magnetic moment of the system. Similar theoretical generalization particularly for ferromagnetism in low and three dimensional organic systems were put forward by some research groups [39, 40]. Ovchinnikov and Spector [39] considered quasi-1D organic polymer ferromagnet having π conjugated carbon chain with a radical attached on every second side carbon. These side radicals (sp^3 centers) were the source of unpaired spins which interact antiferromagnetically with the π electrons (sp^2) and resulted in a net FM organic system. Conjugation effect were shown to result in an increase in the superexchange interaction. Ovchinnikov and Spector [39] also proposed 3D magnetic carbon system with the theoretical magnetization of 230 G g^{-1}. Such systems were called as intermediate graphite diamond structures (IGDS) as they possess mixed hybridisation of sp^3 (diamond) and sp^2 (graphite) carbons. They showed the possible FM interaction among two sp^2 carbon separated by sp^3 carbon due to the net negative value of the exchange integral. Later Fang *et al* [41] also proposed a numerical model for understanding the organic magnets of this kind. They showed FM interaction results from itinerancy of π electrons, electron–electron correlation with π electrons and antiferromagnetic exchange between the π electrons and the unpaired electrons present at the side radicals of quasi 1D organic ferromagnet. Feng *et al* [42] also discussed about the possibility of hopping of the unpaired electrons between its source and the conjugated chain resulting into the high spin state of FM ground state. *Ab initio* method further investigated the details of the kind of exchange interaction between a pair of radicals positioned at sp^2 carbons separated by one or two sp^3 hybridized carbon atoms also suggested the FM exchange coupling [43]. Other magnetic phases like para-, ferri- etc has also been reported for the carbon system with mixed hybridisation states (i.e. sp^2/sp^3 or sp/sp^2) [44–48]. Several such theoretical observations motivated us to experimentally study in details the effect of mixed hybridisation of the carbon atoms on the magnetic property of the system. The most suited carbon system can be GO and rGO because of the easy control of the reaction conditions to accordingly tune the hybridisation of the system. Hence the control over the sp^2 and sp^3 carbon density can help us tune the magnetic property of the possible organic ferromagnets like GO and rGO too. In this paper besides a detailed analysis of the effect of tuning of the hybridization (sp^3 to sp^2 ratio) on the magnetic property of GO and rGO system, we have been keen to understand the possible mechanism of the obtained experimental observations. But before, important parameters to check the sample's purity has been considered exhaustively. Also the sensitive nature of GO and rGO towards the surrounding, measuring instruments and the synthesis protocols have been studied comprehensively [49].

2. Experimental section

2.1. Synthesis of GO and rGO

The synthesis of GO and rGO has been done following the techniques reported in [50–52] (see supplementary information (https://stacks.iop.org/JPCM/33/375801/mmedia) for details). All the chemicals used were purchased from the commercial source (Sigma Aldrich and CDH) and were used without further purification. For the ease of reference, we label the samples prepared under different oxidation conditions as follows: 12 h, 35°C as G1 (least oxidization), 24 h, 50°C as G2 (intermediate oxidation) and 24 h, 65°C as G3 (highest oxidation). Likewise, the three different samples of rGO have been labeled according to the reduction time as follows: 1 min as R1 (least reduction), 40 min as R2 (intermediate reduction) and 80 min as R3 (highest reduction).

Characterization of the synthesized samples were performed using: (a) Rigaku TTRX-III x-ray diffractometer with 1.54 Å Cu-K_α x-ray source using a Bragg-Brentano geometry in a 2θ range of (5°–70°), (b) con-focal micro-Raman spectrometer from Seki Technotron corporation, Japan with 514.5 nm Argon ion laser for Raman studies, (c) Shimadzu IrAffinity-1 for FTIR spectroscopy, (d) ESCA + Omicron Nano Technology GmbH for XPS studies, (e) HRTEM was done using JEOL JEM 2100 PLUS at 200 KeV, (f) Quantum Design Inc. (USA) vibrating sample magnetometer for magnetic measurements.

3. Results and discussions

3.1. Preparation of samples of GO and rGO with different degrees of oxidation

We prepared samples of GO and rGO with three different degrees of oxidation and reduction respectively. Their structural phase has been characterized through XRD, TEM and FTIR. Phase purity of different samples of GO and rGO have been confirmed from XRD as shown in figure 1. Figure 1(a) shows the XRD plot of G2 in the 2θ range of (5°–70°). Signature peak near $2\theta = 9.66°$ (inset figure 1(i)) with no other peaks in this range confirms the structural phase formation of it. XRD plots of G1 and G3 also confirms the absence of impurity peaks [50]. Important structural information dependent upon the variation in the degree of oxidation can be investigated through important peak parameters such as 2θ and the full width at half maximum (FWHM) of the corresponding XRD peak as shown in figure 1(b). They can be obtained using the Lorentzian fitting of the XRD peak using formula $(\frac{A}{(\frac{X-X_0}{\frac{FWHM}{2}})^2+1})$. Figure 1(b) shows the decrease in the 2θ position with increase in the degree of oxidation which implies the increase in the interplanar spacing 'd' between the graphitic sheets (Bragg's law). It is because of the increasing intercalation of the OFGs with increase in the degree of oxidation, showing the increasing fraction of intercalated OFGs from G1 to G3. On the other hand, the FWHM increases with the increase in the structural disorder and the density of point defects in the material [53]. Figure 1(b) shows the monotonic increase in the FWHM with an increasing oxidation indicating the increase in the structural disorder due to the increasing attachment of OFGs. This also confirms that the density of OFGs increases monotonically from G1 to G3. Diffused rings in SAED pattern (inset figure 1(ii)) shows the presence of

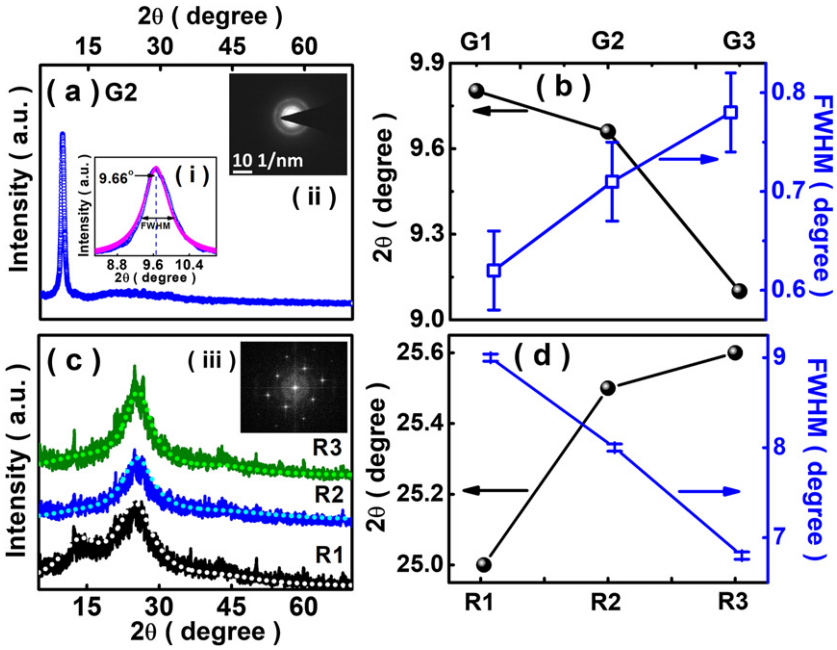

Figure 1. (a) XRD plot of G2 (sample prepared at 24 h, 50°C) with following insets: (i) plot marking the peak location at 9.66° and FWHM obtained from Lorentzian fitting, and (ii) SAED image of G3 (sample prepared at 24 h, 65°C). (b) 2θ (black) and FWHM (blue) variation with oxidation variation in GO obtained from the Lorentzian fitting of the XRD plots of G1 (sample prepared at 12 h, 35°C), G2 and G3 with an error bar of 0.04. (c) XRD plot (along with the Lorentzian fit) of the rGOs with reduction time of R3 (sample prepared at 80 min reduction-green), R2 (sample prepared at 40 min reduction-blue) and R1 (sample prepared at 1 min-black). The additional sharp spikes observed in the XRD are due to noise. (iii) FFT image of R3 (sample prepared at 80 min reduction) showing hexagonal pattern), (d) 2θ (black) and FWHM variations (blue) with reduction time of 1 min, 40 min and 80 min with an error bar of 0.04.

Table 1. XRD analysis of GO and rGO.

S.No.	GO	2θ (degrees)	FWHM (degrees)	d (Å)	rGO	2θ (degrees)	FWHM (degrees)	d (Å)
1	G1	9.802	0.62	9.05	R1	25	9	3.56
2	G2	9.66	0.71	9.16	R2	25.5	8	3.49
3	G3	9.10	0.78	9.74	R3	25.6	6.8	3.47

deformed sheet of GO showing its quasi 2D behavior. Figure 1(c) shows Lorentzian fitted XRD plot of rGO samples, all having a broad peak near the x-ray diffraction angle of $2\theta = 26°$ with no other peaks due to impurities in the range shown confirms their required phase purity [52]. Figure 1(d) shows the variation of 2θ and the FWHM with the reduction time of the samples. Monotonic increase in the 2θ value near 26° with the increasing reduction time indicates the decrease of the interplanar spacing due to the gradual removal of the intercalated OFGs and hence R3 should be the most reduced. Variation of FWHM with the degree of reduction of the samples also affirms it. Decrease in the FWHM with increasing reduction time indicate the decrease in the structural disorder, density of point defects and increase in the crystallinity or sp^2 carbons [53]. Table 1 lists the experimentally obtained values of 2θ, FWHM and d for GO and rGO samples. Figure 1(iii) shows the fast Fourier transformed (FFT) image of R3 having the bright six spots resembling to that of graphene. Removal of OFGs increases the sp^2 fraction of carbon which helps restoration of graphene like structure.

Figure S1(a) (supplementary information) shows the normalised FTIR plot of GO samples (G1, G2 and G3). FTIR fingerprints the elemental composition of the sample (including OFGs) based on the vibrational frequency of the types of bonds present. With the increase in the degree of oxidation, relative variation in the intensity of its FTIR peak is observed accordingly. The peak near 1055 cm^{-1} and 1224 cm^{-1} corresponds to C–O (epoxy) group and the stretching vibration of CHO group respectively with 1616 cm^{-1} corresponding to the bending modes of water molecules. The peak at 1725 cm^{-1} is mainly due to the stretching vibration mode of C=O bonds of the carboxyl or carbonyl groups including ketones and aldehydes [50]. The band near 2900–3500 cm^{-1} can be attributed to the stretching mode of hydroxyl (−OH) groups. The reason for broadness of this peak can be due to the corresponding shifts in its frequencies of vibration with the ranging locations [54]. Figure S1(a) shows that G3 has the maximum intensity for each of the functional groups and G1 showing the least peaks intensity. This supports G1 to be least oxidized and G3 to have the maximum intercalation of OFGs. Figure S1(b) shows the normalised FTIR spectra of the rGO samples. Due to the unique vibrational response of the OFGs, the peak positions and corresponding functional groups hold the similar interpretation for rGO. With increasing reduction, the intensities

of −OH, −C=O, −CHO, C–O–C decreases gradually and hence it also affirms the degree of reduction follows the order as $R3 > R2 > R1$.

3.2. Magnetic signatures in GO and rGO

We observed considerable magnetic moment in GO and rGO samples at 150 K and 300 K and the variation in their magnetic response on the basis of their degree of oxidation and reduction respectively. Figure 2 shows the plot of magnetization (M) versus the applied magnetic field (H) in the range of −10 000 to 10 000 Oe of GO and rGO. At both the temperatures, G1 being the least oxidized is dominated by the diamagnetic (DM) behavior with weak FM effect (inset figures 2(a) and (b)). As the degree of oxidation increases from G2 to G3, magnetic phase shifts from dia- to the combination of para- and FM phases shown in figures 2(a) and (b). Inset figures 2(a) and (b) show the variation in coercivity of samples G2 and G3 such that G3 has more coercivity than G2 at both the temperatures. Similarly, figures 2(c) and (d) shows the M–H plot of rGO at 150 K and 300 K. R3 being the least oxidized has the maximum of DM contribution at 150 K and 300 K respectively. As the degree of reduction decreases, effect on their magnetic phases become obvious as R1 being the least reduced shows more FM contribution than R2 at both 150 K and 300 K. Prominent FM effect can be seen at 150 K in comparison to 300 K for the samples. Inset figures 2(c) and (d) compares their value of coercivity, such that R1 has the maximum value and R3 having the least. In order to investigate the details about the key parameters of the M–H plot like FM saturation magnetisation, coercivity, remanance magnetisation, paramagnetic (PM) or DM susceptibility etc we fit the M–H plot of GO and rGO using an equation

$$M(H) = \left[\frac{2M_{\mathrm{FM}}^{\mathrm{S}}}{\pi}\tan^{-1}\left(\left(\frac{H \pm H_{\mathrm{ci}}}{H}\right)\tan\left(\frac{\pi M_{\mathrm{FM}}^{\mathrm{R}}}{2M_{\mathrm{FM}}^{\mathrm{S}}}\right)\right)\right] + XH \quad (1)$$

referred from [60] as shown in figure 3. The key terms represent experimentally obtained magnetization (M), applied magnetic field (H), FM saturation magnetization ($M_{\mathrm{FM}}^{\mathrm{S}}$), intrinsic coercivity (H_{ci}), FM remanant magnetization ($M_{\mathrm{FM}}^{\mathrm{R}}$), magnetic susceptibility (X) and squareness factor ($K_{\mathrm{p}} = \frac{M_{\mathrm{FM}}^{\mathrm{R}}}{M_{\mathrm{FM}}^{\mathrm{S}}}$). Obtained parameters after fitting them are shown in table 2. With increasing oxidation of GO from 24 h, 50°C to 24 h, 65°C, remanant magnetization, saturation magnetization and coercivity of the FM part has increased at both the temperatures. Similarly, with the increasing reduction, remanant magnetization, saturation magnetization and coercivity has decreased monotonically from R1 to R3. This reveals that degree of oxidation and reduction is playing a vital role in determining the FM contribution. Or may be the density of unpaired spins and their mutual interaction increases with increase in degree of oxidation. Coercivity is found to vary between 100–200 Oe and is comparable to already reported carbon based materials [4, 61]. DM part mainly contribute at 300 K as increase in the temperature results in the increased disorderness in the domain area, resulting in the diminishing of the exchange interaction among the unpaired spins.

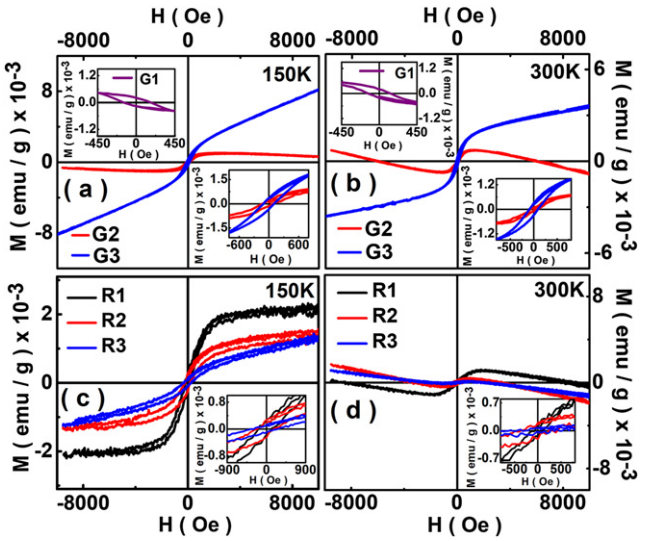

Figure 2. (a) M–H plot of G2 (sample prepared at 24 h, 50°C-red), G3 (sample prepared at 24 h, 65°C-blue) (inset) G1 (sample prepared at 12 h, 35°C (purple) at 150 K (b) M–H plot of G2 (24 h, 50°C-red), G3 (24 h, 65°C-blue) (inset) G1 (12 h, 35°C-purple) at 300 K (c) M–H plot of R1 (sample prepared at 1 min reduction-black), R2 (sample prepared at 40 min reduction-red) and R3 (sample prepared at 80 min reduction-blue) at 150 K (d) M–H plot of R1 (1 min-black), R2 (40 min-red) and R3 (80 min-blue) at 300 K.

Squareness factor (K_{p}) measures the squareness of the hysteresis loop which is 1 for perfect square loop which in our case are small values. Detailed discussion done in next section can help us know how the variation in the degree of oxidation has affected their magnetic property.

3.3. Correlating magnetic signature with the sp^3 to sp^2 carbon content and the I_{D} by I_{G} ratio

In this section we have tried to correlate the observed magnetic signature with the variation in the degree of oxidation and reduction of GO and rGO respectively. We assume that the source of unpaired spins in this carbon based system is the mixture of sp^3 to sp^2 carbons (Ovchinnikov postulation) and the defect density and the variation in them is related to the variation of their magnetic moment and phases. Hence we have tried a detailed analysis of sp^3 to sp^2 carbon ratio and the defect density based on the degree of oxidation and further correlated them with the observed magnetic response.

The chemical states of various elements and the ratio of sp^3 to sp^2 carbon in GO and rGO have been investigated using x-ray photoelectron spectroscopy (XPS). Full scan range (1–1100 eV) XPS plot for GO and rGO shown in inset figures 4(c) and (d) has peaks only for carbon (C1s) and oxygen (O1s), showing the complete absence of any magnetic impurity or d or f electrons. Hence the magnetic response of the system should depend only on the s and p electrons. Figures 4(a)–(c) shows the deconvoluted C1s peaks of R1, R2 and R3. The deconvolution was done using Gaussian–Lorentzian function with the Shirley background on the basis of the theoretical prediction of core level shifts and binding energy

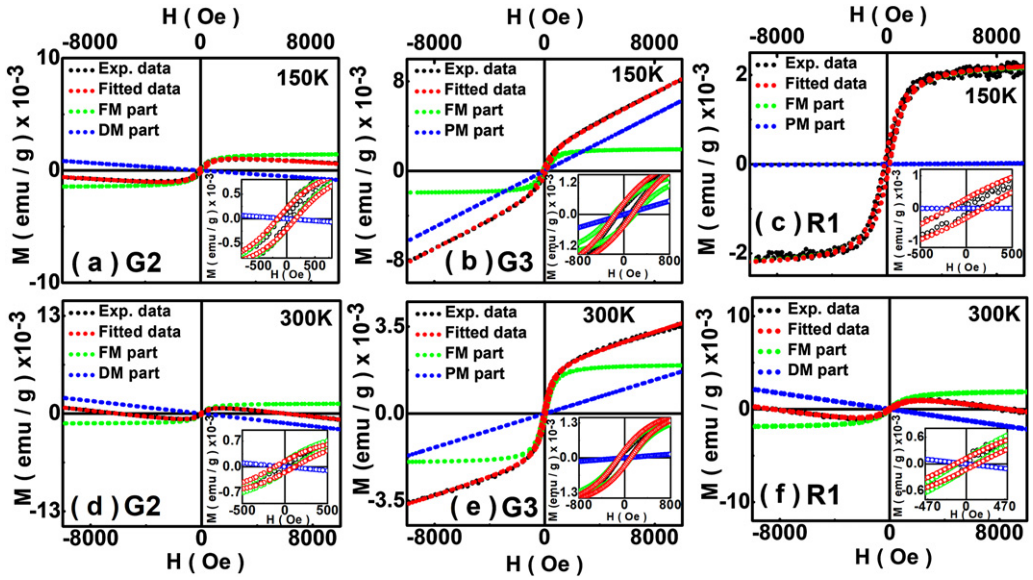

Figure 3. (a) and (d) M–H fitted plot for G2 (24 h, 50°C) at 150 K and 300 K with exp. part (black), fitted part (red), ferromagnetic part (green) and DM part (blue); (b) and (e) M–H fitted plot for G3 (24 h, 65°C) at 150 K and 300 K with exp. part (black), fitted part (red), ferromagnetic part (green) and PM part (blue); (c) and (f) M–H fitted plot of R1 (1 min) at 150 K and 300 K with experimental part (black), fitted part (red), ferromagnetic part (green) and DM/PM part (blue).

Table 2. Parameters obtained after fitting the M–H hysteresis loops of GO and rGO.

S.No.	GO and rGO (150 K)	$M^{R}_{FM} \times 10^{-4}$	$M^{S}_{FM} \times 10^{-3}$	H_{ci}(Oe)	$K_p = \frac{M^{R}_{FM}}{M^{S}_{FM}}$	$X_{para} \times 10^{-6}$
1	G2	2.1	1.5	150	0.14	—
2	G3	4	2.6	193	0.16	1.2
3	R1	2.9	2.3	189	0.12	0.02
4	R2	1.5	1.4	186	0.10	0.02
5	R3	0.8	0.5	183	0.16	0.07
S.No.	GO and rGO (300 K)	$M^{R}_{FM} \times 10^{-4}$	$M^{S}_{FM} \times 10^{-3}$	H_{ci}(Oe)	$K_p = \frac{M^{R}_{FM}}{M^{S}_{FM}}$	$X_{para} \times 10^{-6}$
1	G2	1.5	1.3	100	0.11	—
2	G3	2.9	2.3	120	0.12	0.17
3	R1	1.2	2	113	0.06	—
4	R2	0.9	1.1	109	0.08	—
5	R3	0.5	0.32	106	0.15	—

values of OFGs. This followed deconvolution into five signature peaks located at 284.1 or 283.9 eV (C=C), 284.8 eV (C–C), 286.3 eV (C–O), 288.3 eV (O–C–O/C=O) and 285.8 eV (C–OH) [50]. C–C, C–O, O–C–O/C=O, C–OH contribute to the sp^3 carbon fraction while C=C contribute to the sp^2 ratio. With the increasing reduction time, restoration of C=C has taken place together with the gradual removal of various OFGs. This resulted in the decrease in the sp^3 to sp^2 carbon ratio with increasing reduction. Figures 4(d) and (e) shows the deconvoluted C1s plot of G1 and G2 with signature peak positions same as described above. Details of area under the peaks of G3 has been taken from our previous paper [50]. G1 shows the maximum C=C or sp^2 carbon. As the oxidation time and temperature increased from (24 h, 50°C) to (24 h, 65°C), attachment of OFGs increased resulting in the decrease of sp^2 carbon content. Thus sp^3 to sp^2 ratio is highest for G3 and least for G1. Figure 4(f) combined the variation of sp^3 to sp^2 ratio with the increase and decrease in the oxidation of GO and rGO respectively. Details of area under each peak is given in the tables 3 and 4. We discussed how increase in the degree of oxidation results in an increase in the sp^3 to sp^2 ratio. Now we will see its relation to the defect density of the system. Raman spectroscopy is one of the characterization methods suitable to probe GO and rGO on the basis of structure specific vibrational phonon modes, which is related to the graphitic and the defect density of the system. The prominent Raman peaks of GO and rGO are named as D (near 1340 cm^{-1}), G (near 1580 cm^{-1}) and 2D (near 2700 cm^{-1}) as shown in figures 5(a) and (b) respectively. The defect peak (D peak) arising due to the second order effect involving phonon and defect is due to defects formation within the carbon framework. Chemical functionalization via OFGs and other perturbations like vacancies and adatoms, are considered responsible for the D peak. Broader D peak refer to the higher degree of defects or higher

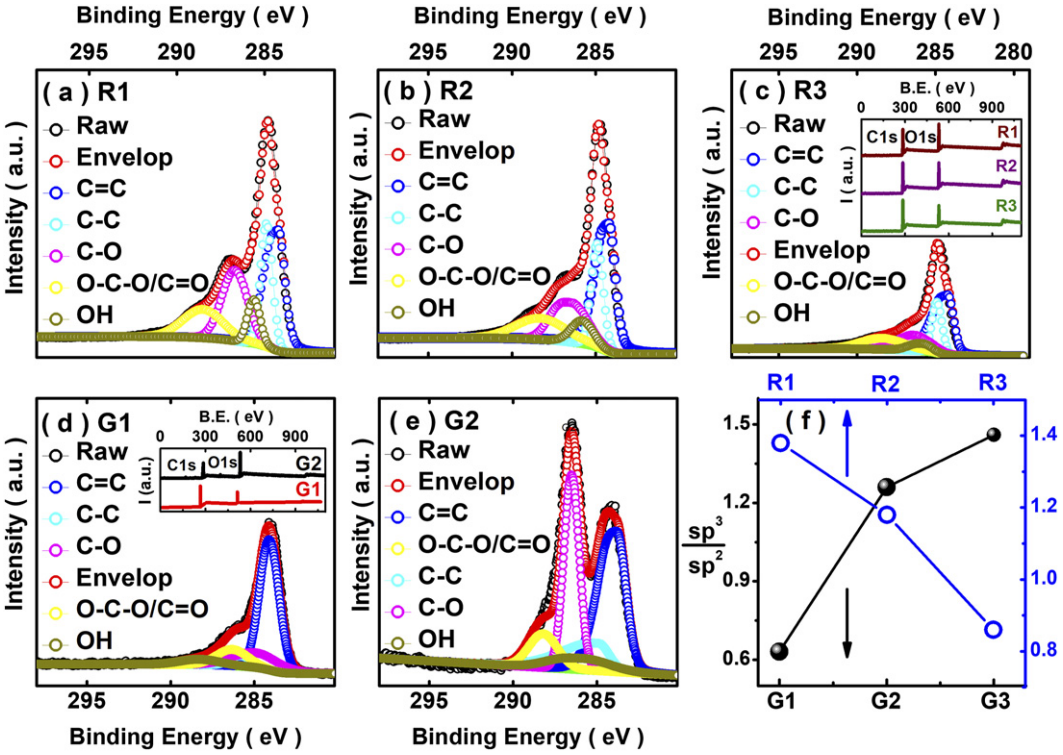

Figure 4. (a)–(e) XPS of C1s peak of R1 (sample prepared at 1 min), R2 (sample prepared at 40 min) and R3 (sample prepared at 80 min), G1 (sample prepared at 12 h, 35°C) and G2 (sample prepared at 24 h, 50°C) into five signature peaks at 283.9/284.1 eV for C=C (blue), 284.9 eV for C–C (magenta), 286.3 eV for C–O (brown), 288.3 eV for O–C–O/C=O (cyan), 285.8 eV for −C–OH (olive) (inset figure (c)) full range XPS plot of rGO (inset figure (d)) full range XPS plot of GO. (f) Variation of sp^3 to sp^2 ratios with increase in degree of oxidation from GO and increase in degree of reduction from rGO.

oxidation [54]. The graphitic peak (G peak) signifies mainly the intact nature of the sp^2 carbon network. The G-peak and the D-peak also represent the in-plane carbon bond stretching and breathing motion of sp^2 carbon pairs respectively. The ratio of area under the D peak to the area under the G peak ($\frac{I_D}{I_G}$) thus measures the relative defects of the carbon framework. As the degree of oxidation increases, defect density is assumed to increase and thus is directly proportional to the sp^3 to sp^2 carbon content. We can see the monotonic increase in the $\frac{I_D}{I_G}$ for the case of GO (figure 5(c)). It means that the increase in the oxygen functionalities causes the increase in the defect density and thus the content of OFGs or sp^3 carbon has increased with $\frac{I_D}{I_G}$ ratio.

On the other hand, $\frac{I_D}{I_G}$ ratio for the rGO series has decreased monotonically with increasing reduction due to the removal of OFGs, showing the reduction in the defect density and the sp^3 carbon density. Table 5 lists the individual values of $\frac{I_D}{I_G}$ ratio of GO and rGO together with their crystallite size $L_a(A^\circ)$. Tunistra and Koenig (TK) studied the Raman spectra of graphite and gave a relation between the defect ratio and the graphite crystallite size. He observed the G-peak position increases with the increase in the defect ratio following the TK equation given below

$$\frac{c(\lambda)}{L_a} = (\frac{I_D}{I_G}), \tag{2}$$

where $c(\lambda)$ equals 44 Å for laser wavelength 514.5 nm. Crystallite size shows an inverse relation with $\frac{I_D}{I_G}$ ratio. The crystallite size decreases with the increase in the defect proportion because of the breakdown of k-selection rule. Finite crystal size activates the A_{1g} vibration mode of the lattice which becomes Raman active and results in the peak near 1355 cm^{-1} [55]. Table 5 shows the increase in the G-peak position with the increasing oxidation and the defect density as observed by TK for graphite. We used TK equation and got the expected lowering of the graphitic crystallite size for both the GO and rGO in the context of the variation in the defect density.

A system can show magnetic property if it has the source of unpaired spins together with exchange interactions like superexchange, direct or indirect exchange forces acting among them. In this section we will try explain how variation of sp^3 to sp^2 carbons and the defect density may results into the variation of unpaired spins and how the exchange interaction operates between them. GO or rGO is a system of conjugated carbon chains with the OFGs attached both at the base and the edges. Oxidation converts a fraction of sp^2 carbons into sp^3 state, such that higher degree of oxidation results into the higher fraction of sp^3 carbons and the defects density. Also we assume that the mixed hybridisation of sp^3 and sp^2 carbons and defects create uncompensated spins and are the source of magnetism in them [56]. Hence attaching OFGs can be considered as an important factor for introducing the local magnetic moment in GO and rGO. Density of OFGs can be tuned by changing the reactor conditions to tune the sp^3 to sp^2 carbon content. This can have control over the magnitude of the spin

Table 3. Fractional area under deconvoluted C1s peaks (GO).

S.No.	GO	283.9/284.1 (eV) (C=C)	284.9 (eV) (C–C)	286.3 (eV) (C–O)	288.3 (eV) (O–C–O/C=O)	285.8 (eV) (C–OH)	$\frac{sp^3}{sp^2}$
1	G3	0.406	0.176	0.218	0.134	0.066	1.46
2	G2	0.440	0.171	0.246	0.078	0.062	1.26
3	G1	0.613	0.164	0.119	0.049	0.052	0.63

Table 4. Fractional area under deconvoluted C1s peaks (rGO).

S.No.	RGO	283.9/284.1 (eV) (C=C)	284.9 (eV) (C–C)	286.3 (eV) (C–O)	288.3 (eV) (O–C–O/C=O)	285.8 (eV) (C–OH)	$\frac{sp^3}{sp^2}$
1	R1	0.425	0.176	0.201	0.130	0.066	1.38
2	R2	0.457	0.155	0.194	0.130	0.062	1.18
3	R3	0.536	0.139	0.138	0.129	0.055	0.86

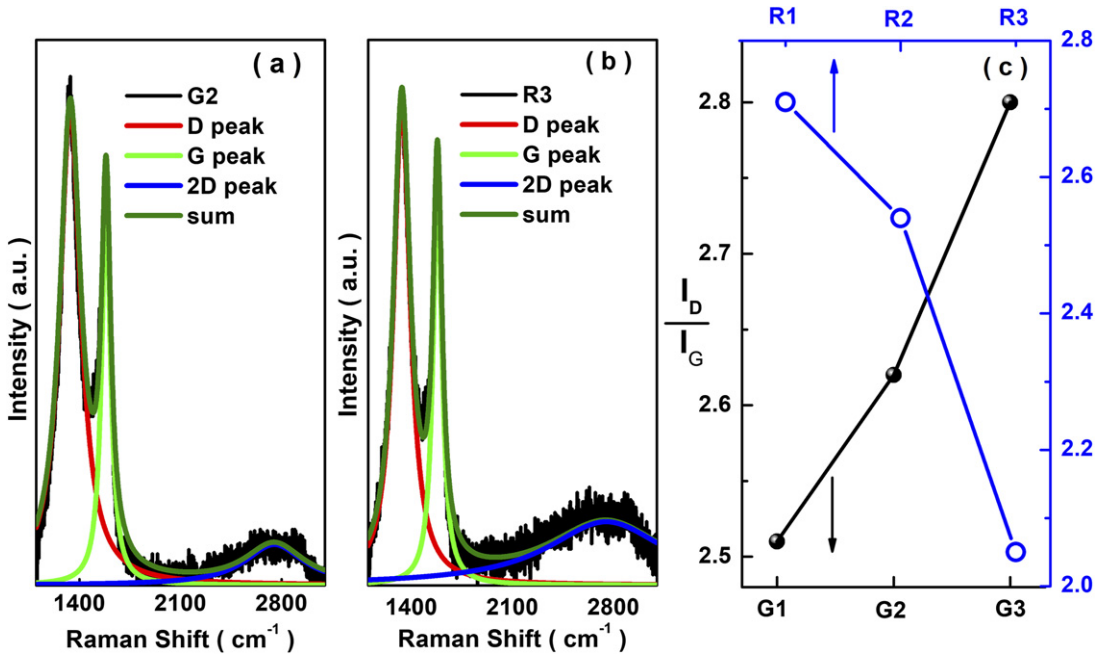

Figure 5. (a) Raman plot of G2 (24 h, 50°C) having the prominent peaks near 1300 cm^{-1} as D peak, 1600 cm^{-1} as G peak and a broad hump in the range of 2500–3000 cm^{-1} named as 2D. (b) Raman plot of R3 (80 min) having the prominent peaks near 1300 cm^{-1} as D peak, 1600 cm^{-1} as G peak and a broad hump in the range of 2500–3000 cm^{-1} named as 2D. (c) Variation of $\frac{I_D}{I_G}$ with increasing oxidation of GO and increasing reduction of rGO.

Table 5. Raman analysis of GO and rGO.

S.No.	GO	G peak (cm^{-1})	$\frac{I_D}{I_G}$	$L_a(A^o)$	rGO	G peak (cm^{-1})	$\frac{I_D}{I_G}$	$L_a(A^o)$
1	G1	1583	2.51	17.5	R1	1585	2.71	16.2
2	G2	1587	2.62	16.7	R2	1583	2.54	17.3
3	G3	1589	2.8	15.7	R3	1581	2.05	21.4

multiplicity and the magnetic phase of the system. It is anticipated that unpaired spins may communicate through the conjugate bonds present on the basal carbon plane such that they align with each other to give the net spin moment to the system. The type of magnetic phases like DM or PM or FM should depend on the sp^3 to sp^2 carbon ratio and defect density. Higher ratio of them has shown the FM contribution and as they gradually decrease, DM contribution enhanced. This quasi 2D system is quite similar to the organic ferromagnet proposed by Ovchinnikov and Spector [39]. They assumed a single chain of sp^2 conjugated carbon atoms and radical R attached to every second side carbon of the chain as a source of unpaired spin.

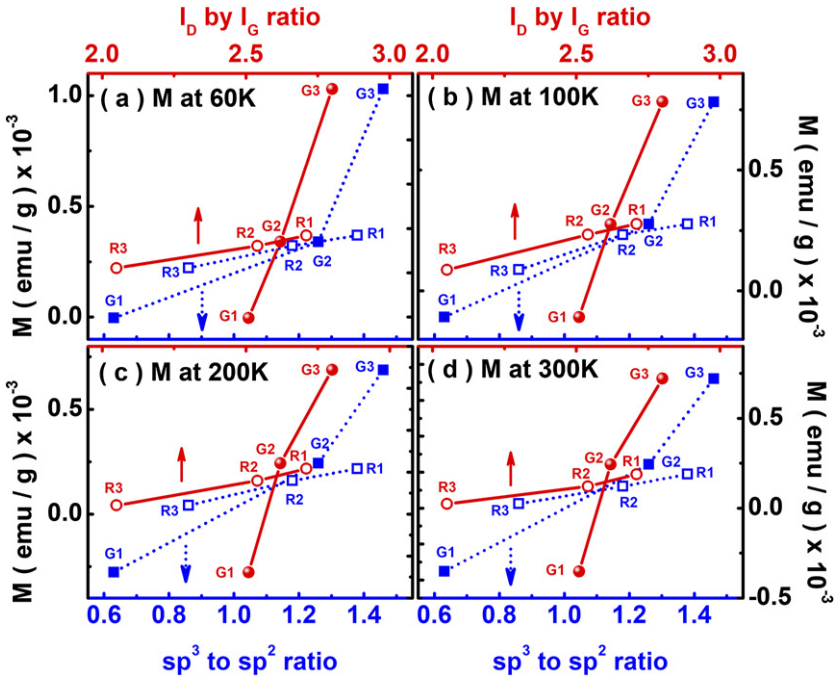

Figure 6. (Bottom X left Y) Increase in magnetic moment with increase in sp^3 to sp^2 ratios of G1 (12 h, 35°C), G2 (24 h, 50°C) and G3 (24 h, 65°C) and R3 (80 min), R2 (40 min) and R1 (1 min) at different temperatures ((a) 60 K, (b) 100 K, (c) 200 K, (d) 300 K); (top X right Y) variation of magnetic moment with I_D by I_G ratio of GO and rGO.

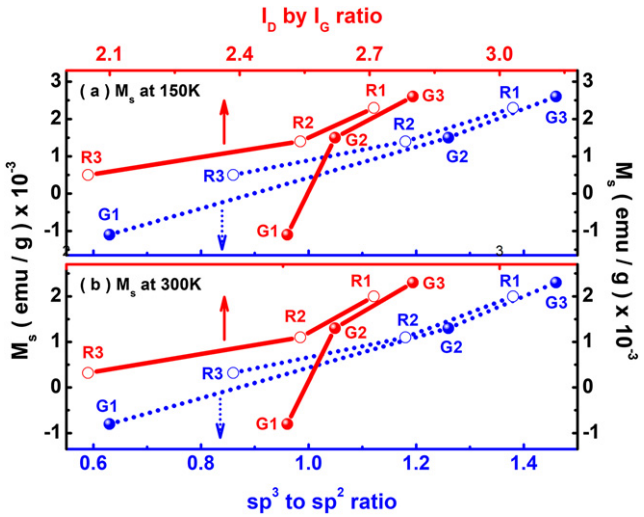

Figure 7. (Bottom X left Y) Increase in saturation magnetization with increase in sp^3 to sp^2 ratios from G1 (12 h, 35°C), G2 (24 h, 50°C) to G3 (24 h, 65°C) and R3 (80 min), R2 (40 min) and R1 (1 min); (top X right Y) variation of saturation magnetization with respect to I_D by I_G ratio of GO and rGO.

The carbon to which R gets attached converts its hybridization from sp^2 to sp^3. Hence the system becomes a combination of sp^2 and sp^3 carbons. Such system were theoretically shown to be FM. Since practically organic ferromagnets need not contain only single chain rather multiple dimers can exist with the possibility that each main chain gets coupled with each other. In these cases interchain coupling factor comes into play. Theoretical models of the interchain coupling of the chain was also studied via SSH Hamiltonian [57], Hamiltonian including Hubbard electron–electron repulsion and nearest neighbor Coulomb repulsion [58] and interchain electron transfer using mean field approximation [59]. Each of the models supported the possibility of the FM ordering at ground state. These theoretical models strictly followed the structure of polymer as of alternate sp^2 and sp^3 carbons which practically seems not easy. In our case, GO and rGO can be considered as multi π conjugated chain coupled with each other via electron bonding and each chain consist the variable number of R radicals as a source of unpaired spins. R radicals in our case are OFGs which converts the carbon hybridization from sp^2 to sp^3 resulting into a mixture of sp^2 and sp^3 carbons. As the density of OFGs or the sp^3 to sp^2 carbon ratio is tuned from low to high, magnetic property seems to follow the magnetic phase transition from DM, PM to FM for both GO and rGO. We assume that when sp^2 to sp^3 carbon ratio is high, it result into the high unpaired spin density. These unpaired spins interact with each other via π electrons thus increasing the intermediate exchange force. This overall result into the long range exchange interaction and FM phase. As the sp^3 to sp^2 carbons or source of unpaired spins decrease together with the decrease in defect density due to OFGs, magnitude of exchange interaction decreases. And for the least number sp^3 to sp^2 carbons, where the conjugation effect may become prominent due to the restoration of sp^2 carbons but the number of unpaired spins is not sufficient to introduce spin–spin interaction. Spins cannot talk to each other due to weak or no exchange interaction. And hence do not respond to the external applied magnetic field. In summary, G1 has the least density of OFGs or the sp^3 carbons and possess the DM phase at both 150 K and 300 K. G2 being intermediately oxidized show combination of FM and weak DM

property at both the temperatures. G3 shows the combination of FM and PM property with no diamagnetism remains at both 150 K and 300 K. Similar observations are for rGO. R1 having the highest density of OFGs has the highest FM contribution and R3 being the highly reduced has maximum contribution of DM part.

Figure 6 shows the individual variation of the magnetic moment with respect to the degree of oxidation and reduction (or sp^3 to sp^2 ratio) and the I_D by I_G ratio at different temperatures. With the increase in oxidation of the GO sets, magnetic moment has increased due to the increase in the density of unpaired spins resulting from mixed hybridized states and the defect density. Similarly, magnetic moment has decreased with increased reduction time for rGO. Hence both the systems (GO and rGO) supports that the density of sp^3 carbons and defects are the source of magnetic moment in a them and the degree of oxidation affects their magnetic phase. Figure 7 shows the variation of the saturation magnetization with the increase in sp^3 to sp^2 ratio and I_D by I_G ratio. In case of GO, with the increase in the sp^3 to sp^2 and I_D by I_G ratio, the saturation magnetization monotonically increases and G3 has the maximum FM part. The similar behavior is seen for rGO. As reduction time increases till 80 min, the saturation magnetization has followed the monotonic decrease and hence R1 has highest FM contribution in comparison to R2 and R3.

It is worthwhile to comment here that the defects arising due to the attachment of OFGs and the sp^3 to sp^2 carbon ratio are interrelated. The comparison of magnetization data (including the saturation magnetization values) as a function of $sp^3 : sp^2$ and $I_D : I_G$ ratios (see figures 6 and 7) illustrates this point. Further work in this direction (both experimental and theoretical) is required for a detailed understanding of the underlying mechanism.

We summarize that the carbon based systems like GO and rGO which lacks d or f electrons, transition metal doping or magnetic impurities, can also show magnetic property. In GO and rGO, the density and type of OFGs determine the magnitude of magnetic moment and the magnetic phases. Such system behave similar to the Ovchinnikov magnet as they are similar to IGDS as proposed by Ovchinnikov and Spector [39] and in future can be used as 'organic' magnetic layers in suitable devices. The conjugation effect may help increase the magnetization due to an increase in coupling effect (such as superexchange coupling, etc).

4. Conclusion

We have studied the magnetic response of a set of samples of GO and rGO with a systematic variation in the sp^3 to sp^2 ratio of carbon. XRD, FTIR, Raman spectroscopy and XPS measurements has supported the structural and compositional phase purity of the material as well as to the designed variation of the sp^3 to sp^2 carbon ratio with the changing degree of oxidation. We observe a systematic variation in their magnetic moment with the degree of oxidation and reduction. The net moment of the system depends sp^3 to sp^2 carbon ratio and thus on the density of OFGs. Increase in sp^3 carbons results in more localized states and corresponding increase of magnetic moment; this has been corroborated for both GO and rGO samples. This system thus resembles the IGDS as proposed by Ovchinnikov. Both has the mixed densities of sp^3 and sp^2 carbons such that sp^3 carbons may be one of the factors for the source of unpaired spins in analogy to the IGDS; an exchange interaction between the π electrons due to sp^2 carbons and the unpaired electrons due to sp^3 states leads to the net magnetic moment of the system. A similar phenomena was at the heart of the proposal of Ovchinnikov organic ferromagnets. The tunability of magnetic response based on the sp^3/sp^2 fraction makes GO and its derivatives as a potential Ovchinnikov ferromagnet candidate that can be utilized in carbon based spintronic applications.

Acknowledgments

AS would like to thank UGC (India) for their financial support.

Data availability statement

All data that support the findings of this study are included within the article (and any supplementary files).

ORCID iDs

Ajay D Thakur https://orcid.org/0000-0002-8941-7763

References

[1] Hong J, Bekyarova E, Liang P, de Heer W A, Haddon R C and Khizroev S 2012 Room-temperature magnetic ordering in functionalized graphene *Sci. Rep.* **2** 624
[2] Sepioni M, Nair R R, Rablen S, Narayanan J, Tuna F, Winpenny R, Geim A K and Grigorieva I V 2010 Limits on intrinsic magnetism in graphene *Phys. Rev. Lett.* **105** 207205
[3] Wang Y, Huang Y, Song Y, Zhang X, Ma Y, Liang J and Chen Y 2009 Room-temperature ferromagnetism of graphene *Nano Lett.* **9** 220
[4] Rao S S, Jammalamadaka S N, Stesmans A, Moshchalkov V V, van Tol J, Kosynkin D V, Higginbotham-Duque A and Tour J M 2012 Ferromagnetism in graphene nanoribbons: split versus oxidative unzipped ribbons *Nano Lett.* **12** 1210
[5] Sahin H, Senger R T and Ciraci S 2010 Spintronic properties of zigzag-edged triangular graphene flakes *J. Appl. Phys.* **108** 074301
[6] Vittorio O, Duce S L, Raffa V and Cuschieri A 2011 Imaging and biomedical application of magnetic carbon nanotubes *Carbon Nanotubes: Growth and Applications* ed N Mohammad (London: IntechOpen) https://doi.org/10.5772/16633
[7] Siddiqui M T H *et al* 2019 Fabrication of advance magnetic carbon nano-materials and their potential applications: a review *J. Environ. Chem. Eng.* **7** 1028122
[8] Ma J, Zhu Z, Chen B, Yang M, Zhou H, Li C, Yu F and Chen J 2013 One-pot, large-scale synthesis of magnetic activated carbon nanotubes and their applications for arsenic removal *J. Mater. Chem.* A **1** 4662
[9] Abdi G, Alizadeh A, Zinadini S and Moradi G 2018 Removal of dye and heavy metal ion using a novel synthetic

polyethersulfone nanofiltration membrane modified by magnetic graphene oxide/metformin hybrid *J. Membr. Sci.* **552** 326
[10] Höhne R and Esquinazi P 2002 Can carbon Be ferromagnetic? *Adv. Mater.* **14** 753
[11] Yazyev O V 2010 Emergence of magnetism in graphene materials and nanostructures *Rep. Prog. Phys.* **73** 056501
[12] Li J *et al* 2020 Preparing dangling bonds by nanoholes on graphene oxide nanosheets and their enhanced magnetism *RSC Adv.* **10** 36378
[13] Ionov A N, Volkov M P, Nikolaeva M N, Smyslov R Y and Bugrov A N 2021 Magnetization of ultraviolet-reduced graphene oxide flakes in composites based on polystyrene *Materials* **14** 2519
[14] Khurana G, Kumar N, Kotnala R K, Nautiyal T and Katiyar R S 2013 Temperature tuned defect induced magnetism in reduced graphene oxide *Nanoscale* **5** 3346
[15] Darminto D *et al* 2018 Enhanced magnetism by temperature induced defects in reduced graphene oxide prepared from coconut shells *IEEE Trans. Magn.* **54** 1600105
[16] Yan J-A and Chou M Y 2010 Oxidation functional groups on graphene: structural and electronic properties *Phys. Rev.* B **82** 125403
[17] Carpio A, Bonilla L L, de Juan F and Vozmediano M A H 2008 Dislocations in graphene *New J. Phys.* **10** 053021
[18] Ćirić L, Djokić D M, Jaćimović J, Sienkiewicz A, Magrez A, Forró L, Šljivančanin Z, Lotya M and Coleman J N 2012 Magnetism in nanoscale graphite flakes as seen via electron spin resonance *Phys. Rev.* B **85** 205437
[19] Kundu A and Zhang S 2015 Temperature dependence of RKKY interaction *J. Magn. Magn. Mater.* **393** 331
[20] Govind Raj K and Joy P A 2014 Ferromagnetism at room temperature in activated graphene oxide *Chem. Phys. Lett.* **605–606** 89
[21] Tang T, Tang N, Zheng Y, Wan X, Liu Y, Liu F, Xu Q and Du Y 2015 Robust magnetic moments on the basal plane of the graphene sheet effectively induced by OH groups *Sci. Rep.* **5** 8448
[22] Santos E J G, Ayuela A and Sánchez-Portal D 2012 Universal magnetic properties of sp^3-type defects in covalently functionalized graphene *New J. Phys.* **14** 043022
[23] Sun Y, Zheng Y, Chen J, Zhang W, Tang N and Du Y 2016 Intrinsic magnetism of monolayer graphene oxide quantum dots *Appl. Phys. Lett.* **108** 033105
[24] Lehtinen P O, Foster A S, Ayuela A, Krasheninnikov A, Nordlund K and Nieminen R M 2003 Magnetic properties and diffusion of adatoms on a graphene sheet *Phys. Rev. Lett.* **91** 017202
[25] Singh R and Kroll P 2009 Magnetism in graphene due to single-atom defects: dependence on the concentration and packing geometry of defects *J. Phys.: Condens. Matter* **21** 196002
[26] Tadyszak K, Scheibe B, Ostrowski A, Musiał A and Wychowaniec J K 2021 Influence of thermochemical reduction on magnetic properties of reduced graphene oxide aerogels *J. Phys. Chem. Solids* **151** 109898
[27] Boukhvalov D W 2011 Repair of magnetism in oxidized graphene nanoribbons *Chem. Phys. Lett.* **501** 396
[28] Augustyniak-Jabłokow M A, Carmieli R, Strzelczyk R, Fedaruk R and Tadyszak K 2021 Electron spin echo studies of hydrothermally reduced graphene oxide *J. Phys. Chem.* C **125** 4102
[29] Lee D, Seo J, Zhu X, Cole J M and Su H 2015 Magnetism in graphene oxide induced by epoxy groups *Appl. Phys. Lett.* **106** 172402
[30] Qin S, Guo X, Cao Y, Ni Z and Xu Q 2014 Strong ferromagnetism of reduced graphene oxide *Carbon* **78** 559
[31] Tajima K, Isaka T, Yamashina T, Ohta Y, Matsuo Y and Takai K 2017 Functional group dependence of spin magnetism in graphene oxide *Polyhedron* **136** 155
[32] Wang M and Li C M 2010 Magnetism in graphene oxide *New J. Phys.* **12** 083040
[33] Sherafati M and Satpathy S 2011 Analytical expression for the RKKY interaction in doped graphene *Phys. Rev.* B **84** 125416
[34] Wang M, Huang W, Chan-Park M B and Li C M 2011 Magnetism in oxidized graphenes with hydroxyl groups *Nanotechnology* **22** 105702
[35] Bagani K, Ray M K, Satpati B, Ray N R, Sardar M and Banerjee S 2014 Contrasting magnetic properties of thermally and chemically reduced graphene oxide *J. Phys. Chem.* C **118** 13254
[36] Sarkar S K, Raul K K, Pradhan S S, Basu S and Nayak A 2014 Magnetic properties of graphite oxide and reduced graphene oxide *Physica* E **64** 78
[37] Kim S-W, Kim H-K, Lee K, Roh K C, Han J T, Kim K-B, Lee S and Jung M-H 2019 Studying the reduction of graphene oxide with magnetic measurements *Carbon* **142** 373
[38] Arun T *et al* 2021 Role of electrolytes on the electrochemical characteristics of Fe_3O_4/MXene/RGO composites for supercapacitor applications *Electrochim. Acta* **367** 137473
[39] Ovchinnikov A A and Spector V N 1988 Organic ferromagnets. New results *Synth. Met.* **27** 615
[40] Teki Y, Takui T, Itoh K, Iwamura H and Kobayashi K 1986 Preparation and ESR detection of a ground-state nonet hydrocarbon as a model for one-dimensional organic ferromagnets *J. Am. Chem. Soc.* **108** 2147
[41] Fang Z, Liu Z L and Yao K L 1994 Theoretical model and numerical calculations for a quasi-one-dimensional organic ferromagnet *Phys. Rev.* B **49** 3916
[42] Fang Z, Liu Z L and Yao K L 1995 *The 40th Conf. Magnetism and Magnetic Materials*
[43] Ovchinnikov A A, Shamovsky I L and Bozhenko K V 1991 *Ab initio* molecular orbital studies on a singlet-triplet splitting of C_3H_6 and C_4H_8 molecules *J. Mol. Struct.* **251** 141
[44] Tuček J, Błonski P, Ugolotti J, Swain A K, Enokib T and Zbořil R 2018 Emerging chemical strategies for imprinting magnetism in graphene and related 2D materials for spintronic and biomedical applications *Chem. Soc. Rev.* **47** 3899
[45] Ovchinnikov A A and Shamovsky I L 1991 The structure of the ferromagnetic phase of carbon *J. Mol. Struct.* **251** 133
[46] Arčon D, Jagličič Z, Zorko A, Rode A V, Christy A G, Madsen N R, Gamaly E G and Luther-Davies B 2006 Origin of magnetic moments in carbon nanofoam *Phys. Rev.* B **74** 014438
[47] Zheng Y, Chen Y, Lin L, Sun Y, Liu H, Li Y, Du Y and Tang N 2017 Intrinsic magnetism of graphdiyne *Appl. Phys. Lett.* **111** 033101
[48] Yu G, Liu Z, Gao W and Zheng Y 2013 Electronic properties of four typical zigzag-edged graphyne nanoribbons *J. Phys.: Condens. Matter* **25** 285502
[49] Sinha A, Ranjan P and Thakur A D 2021 Effect of characterization probes on the properties of graphene oxide and reduced graphene oxide (to be published)
[50] Ranjan P, Agrawal S, Sinha A, Rao T R, Balakrishnan J and Thakur A D 2018 A low-cost non-explosive synthesis of graphene oxide for scalable applications *Sci. Rep.* **8** 12007
[51] Marcano D C, Kosynkin D V, Berlin J M, Sinitskii A, Sun Z, Slesarev A, Alemany L B, Lu W and Tour J M 2010 Improved synthesis of graphene oxide *ACS Nano* **4** 4806

[52] Abdolhosseinzadeh S, Asgharzadeh H and Kim H S 2015 Fast and fully-scalable synthesis of reduced graphene oxide *Sci. Rep.* **5** 10160
[53] Vashista M and Paul S 2012 Correlation between full width at half maximum (FWHM) of XRD peak with residual stress on ground surfaces *Phil. Mag.* **92** 33
[54] Dimiev A M 2016 Mechanism of formation and chemical structure of graphene oxide *Graphene Oxide: Fundamentals and Applications Print* ed A M Dimiev and S Eigler (New Jersey: Wiley)
[55] Tuinstra F and Koenig J L 1970 Raman spectrum of graphite *J. Chem. Phys.* **53** 1126
[56] Majchrzycki Ł, Augustyniak-Jabłokow M A, Strzelczyk R and Maćkowiak M 2015 Magnetic centres in functionalized graphene *Acta Phys. Pol.* A **127** 2
[57] Wang W Z, Yao K L and Lin H Q 1997 A theoretical model for interchain coupled organic ferromagnets *Chem. Phys. Lett.* **274** 221
[58] Wang W Z and Yao K L 1997 A study on the ground state in interchain coupled quasi-one-dimensional organic ferromagnets *J. Phys.: Condens. Matter* **9** 6931
[59] Li H-T 1997 Interchain interaction in quasi-one-dimension organic polymer ferromagnets *Mod. Phys. Lett.* B **11** 821
[60] Duhalde S *et al* 2005 Appearance of room-temperature ferromagnetism in Cu-doped $TiO_{2-\delta}$ films *Phys. Rev.* B **72** 161313
[61] Esquinazi P, Höhne R, Han K-H, Setzer A, Spemann D and Butz T 2004 Magnetic carbon: explicit evidence of ferromagnetism induced by proton irradiation *Carbon* **42** 1213